ADVANCED MATERIALS
www.advmat.de

Transparent and Freestanding Single-Walled Carbon Nanotube Films Synthesized Directly and Continuously via a Blown Aerosol Technique

Qiang Zhang, Weiya Zhou, Xiaogang Xia, Kewei Li, Nan Zhang, Yanchun Wang, Zhuojian Xiao, Qingxia Fan, Esko I. Kauppinen, and Sishen Xie**

Single-walled carbon nanotube (SWCNT) films are promising materials as flexible transparent conductive films (TCFs). Here, inspired by the extrusion blown plastic film technique and the SWCNT synthesis approach by floating catalyst chemical vapor deposition (FCCVD), a novel blown aerosol chemical vapor deposition (BACVD) method is reported to directly and continuously produce freestanding SWCNT TCFs at several hundred meters per hour. The synthesis mechanism, involving blowing a stable aerosol bubble and transforming the bubble into an aerogel, is investigated, and a general phase diagram is established for this method. For the SWCNT TCFs via BACVD, both carbon conversion efficiency and SWCNT TCF yield can reach three orders of magnitude higher than those with the conventional FCCVD. The film displays a sheet resistance of 40 ohm sq^{-1} at 90% transmittance after being doped, representing the record performance based on large-scale SWCNT films. Transparent, flexible, and stretchable electrodes based on BACVD films are demonstrated. Moreover, this high-throughput method of producing SWCNT TCFs can be compatible with the roll-to-roll process for mass production of flexible displays, touch screens, solar cells, and solid-state lighting, and is expected to have a broad and long-term impact on many fields from consumer electronics to energy conversion and generation.

Transparent conductive electrodes have pervaded modern technologies since they represent an essential component of various optoelectronic devices. Currently, indium tin oxide (ITO) is the most widely used transparent conductive material.[1] The brittle nature and the limited resource of indium, however, present many challenges for ITO applications in flexible electronics. Therefore, alternative transparent conductive materials, e.g., carbon nanotubes (CNTs),[2–4] graphene,[5] metal nanowires,[6] and metal meshes,[7] have received extensive attention. Among these promising candidates, single-walled carbon nanotube (SWCNT) transparent conductive films (TCFs) exhibit great potential because of their outstanding electrical, optical, and mechanical properties, good flexibility, and high environmental stability.[8] The main methods for production of transparent SWCNT films include liquid-phase processing and floating catalyst chemical vapor deposition (FCCVD).[3] Although the solution-based film fabrication is readily scalable and low-cost, the CNT dispersion process can inevitably lead to contamination and shortening of the nanotubes, thus reducing the performance of a film. Compared with the liquid-phase processing, the FCCVD is more direct and simpler, avoiding the sonication in solution as well as the use of surfactants. Nevertheless, the current fabrication of CNT films based on FCCVD requires multiple procedures mainly including CNT synthesis, gas filtration, and press transfer.[4] Furthermore, these methods of SWCNT transparent electrodes are not compatible with high-throughput production which should preferably be performed in a continuous process such as roll-to-roll processing. Here, inspired by the

Dr. Q. Zhang, Prof. W. Y. Zhou, X. G. Xia, K. W. Li, Dr. N. Zhang, Dr. Y. C. Wang, Dr. Z. J. Xiao, Dr. Q. X. Fan, Prof. S. S. Xie
Beijing National Laboratory for Condensed Matter Physics
Institute of Physics
Chinese Academy of Sciences
Beijing 100190, China
E-mail: wyzhou@iphy.ac.cn; ssxie@iphy.ac.cn

Dr. Q. Zhang, Prof. W. Y. Zhou, X. G. Xia, K. W. Li, Dr. N. Zhang, Dr. Z. J. Xiao, Dr. Q. X. Fan, Prof. S. S. Xie
University of Chinese Academy of Sciences
Beijing 100049, China

Prof. W. Y. Zhou, Dr. Y. C. Wang, Prof. S. S. Xie
Beijing Key Laboratory for Advanced Functional Materials and Structure Research
Beijing 100190, China

Prof. W. Y. Zhou, Prof. S. S. Xie
Songshan Materials Laboratory
Guangdong, Dongguan 523808, China

Prof. E. I. Kauppinen
Department of Applied Physics
Aalto University School of Science
Espoo FI-00076, Finland

The ORCID identification number(s) for the author(s) of this article can be found under https://doi.org/10.1002/adma.202004277.

DOI: 10.1002/adma.202004277

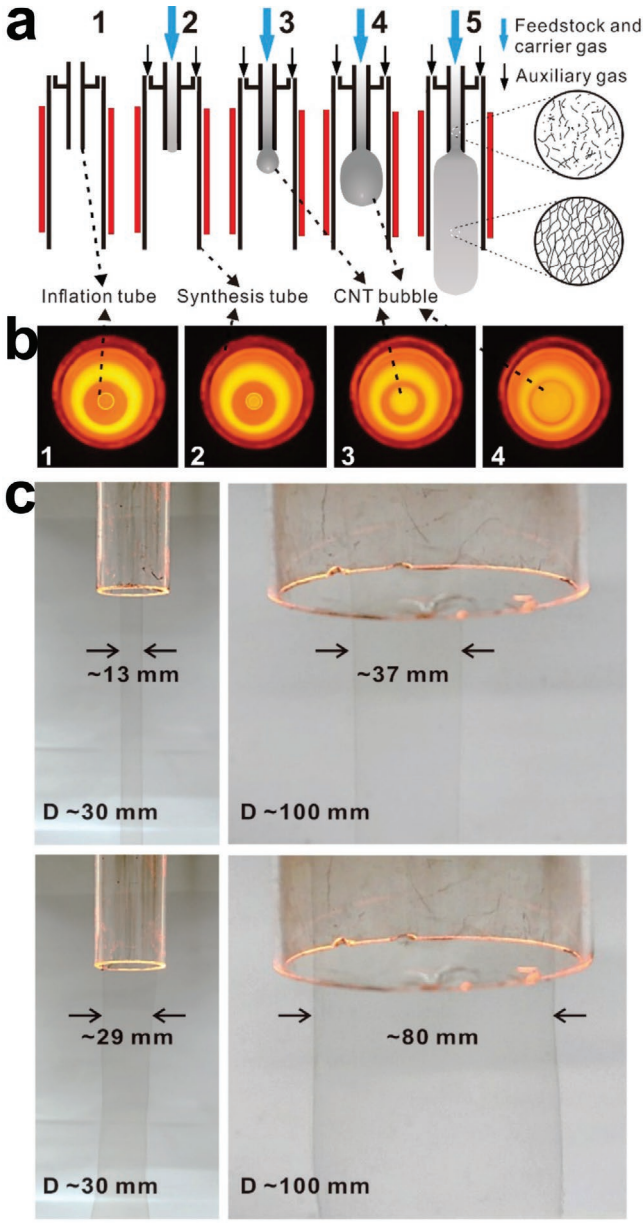

Figure 1. The equipment and process of a freestanding CNT film synthesized by BACVD. a) Schematic showing the fabrication process of a tubular CNT film by BACVD. The aerosol containing CNTs is formed in the inflation tube and blown into a bubble at the inflation tube outlet. In the synthesis tube, the bubble, with CNT growing further, is transformed from aerosol into aerogel and grows up. b) Real-time bottom views of a CNT bubble forming in Equipment #2, corresponding to the processes from 1 to 4 in Figure 1a, respectively. c) Optical images of the freestanding tubular CNT films with different diameters blown from Equipment #1 (left, the synthesis tube of ≈30 mm in diameter) and Equipment #2 (right, the synthesis tube of ≈100 mm in diameter), corresponding to the process 5 in Figure 1a.

extrusion blown plastic film technique[9,10] and the CNT synthesis via FCCVD,[11,12] we have developed a new approach to directly and continuously produce a high-quality, freestanding, and transparent conductive SWCNT film with an ultrahigh yield. Basically, this approach introduces a blown CNT aerosol technique into the FCCVD process of the CNT synthesis, which we term as blown aerosol chemical vapor deposition (BACVD). Especially, BACVD technique of producing continuous and freestanding CNT film fabrication is compatible with the general roll-to-roll process.

Schematic and photographs of the equipment and process of a freestanding CNT film synthesized by BACVD method are shown in **Figure 1**. The reactor consists of a vertical furnace and two coaxial quartz tubes, an "inflation tube" inside a "synthesis tube". The outlet of the inflation tube for blowing the CNT aerosol is located in the high-temperature zone (Figure 1a and Figure S1, Supporting Information), which is critical for the preparation of a continuous and homogeneous film. In addition, at the top of the synthesis tube, there is an inlet of auxiliary gas for removing residual air and adjusting the gas pressure. Feedstock for CNT synthesis, carrier gas for the aerosol inflation (Video S1, Supporting Information), and a small flow of auxiliary gas are introduced continuously (Figure S1, Supporting Information). By this means, tubular thin CNT films are continuously blown out from the outlet of the synthesis tube (Figure 1c and Videos S2–S4, Supporting Information). The blow-out speed of the tubular film by BACVD is 50–600 m h^{-1}. This design hence combines the blown aerosol technique with the FCCVD process. To demonstrate the scalability of this method, two sets of equipment (#1 and #2) with different scales were built as described in detail in the Experimental Section and in Section S1, Supporting Information. Subsequent discussion is based on the large-scale equipment #2, with a synthesis tube of 10 cm in diameter, unless otherwise specified.

BACVD differs in mechanism from the improved CVD methods used previously to grow CNTs, especially in terms of CNT assembly. Systematic investigation of various combinations of synthesis conditions and their corresponding products reveals that two critical processes (C1 and C2) are involved in tubular film fabrication. In process C1, a stable aerosol bubble is blown while process C2 transforms the bubble from an aerosol into an aerogel. The SWCNTs in C1 aerosol have some interaction,[11,13] which is different in the general aerosol,[14] and could be transformed under a suitable condition into SWCNT aerogel in C2 as a final product.[13,15] BACVD essentially combines a blowing SWCNT-aerosol technique with FCCVD for CNT synthesis.

The blowing bubble process is shown in Figure 1b and Video S1, Supporting Information. During the feedstock decomposition and CNT growth, an aerosol containing the growing CNTs with weak interactions is formed in the inflation tube. The aerosol is then blown into a bubble at the inflation tube outlet. In the synthesis tube, the aerosol bubble expands to a certain diameter, depending on the balance between the gas pressure difference and the bubble strength. The CNTs grow continuously throughout this process. The bubble with elongating nanotubes can be transformed from an aerosol into an aerogel, that is, a continuous and robust network is formed. In this process, the direct connection between the inflation tube and the CNT bubble is beneficial for the preparation of a stable and uniform tubular film.

A general phase diagram of CNTs synthesized by BACVD was determined and the corresponding products were

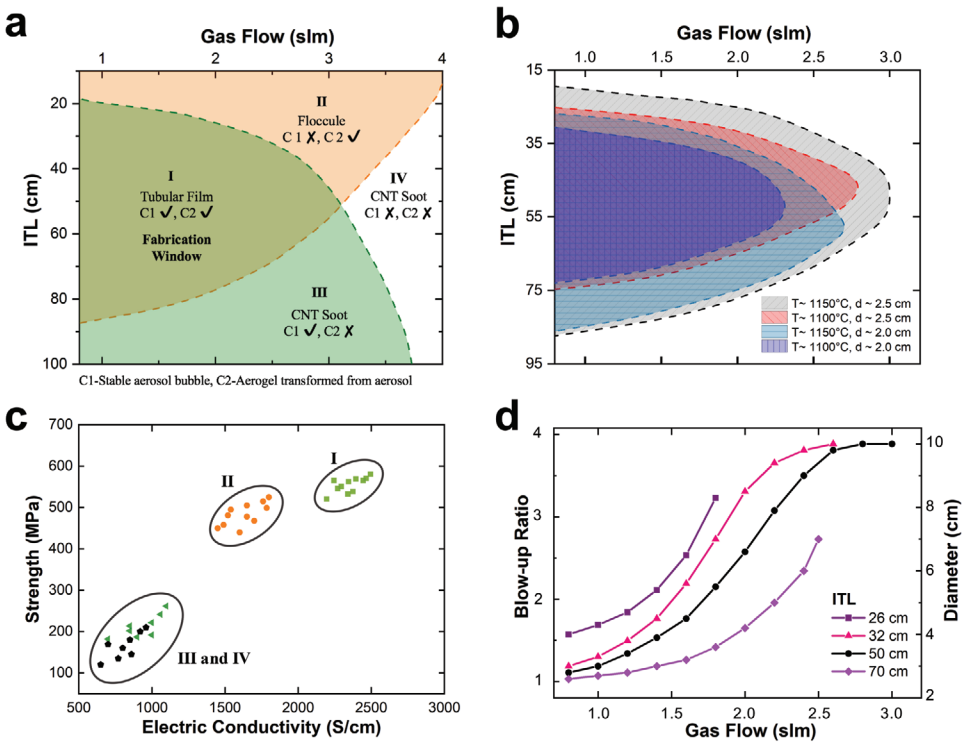

Figure 2. Film formation mechanism of BACVD. a) Phase diagram of the CNT synthesis in Equipment #2. Four phase regions based on processes C1 and C2 are indicated. Inflation tube diameter (d) ≈ 25 mm and furnace temperature (T) ≈ 1150 °C. b) Fabrication windows of tubular films, which shrink with lowing T or decreasing d. c) Conductivity and mechanical strength of the CNT products in each phase region. The tubular films display excellent performance. Compared with the tubular films or CNT floccule films, the properties of the films consisting of CNT soot are significantly inferior. d) The relation between the blow-up ratio of a film and the carrier gas flow with various ITLs in Equipment #2. The inflation tubes have the same size of d ≈ 25 mm.

characterized, as shown in **Figure 2**a and Section S2, Supporting Information. The synthesis temperature (T) was ≈1150 °C and the temperature profile of the reactor is shown in Figure S1, Supporting Information. The phase diagram is divided into four regions; the orange and cyan regions (II and III) represent the conditions satisfying processes C1 and C2, respectively. Their overlapping region I is the "fabrication window" in which both processes are successful and the synthesis conditions are suitable for the fabrication of continuous tubular films. In the other three phase regions failure of C1 or C2 takes place, and the corresponding CNT products may be in a flocculent or sooty state, depending on the carrier gas flow and inflation tube length (ITL) within the synthesis tube. We also studied the influence of T and inflation tube diameter (d) on the fabrication window. As shown in Figure 2b, decreasing the T or d shrinks this window. The temperature has a pronounced influence on both the C1 and C2 processes, while d mainly affects C1. More discussion about the effect of synthesis conditions on the fabrication window is in Section S3, Supporting Information.

The CNT products corresponding to each phase region and their properties were characterized (Figure 2c and Section S2, Supporting Information). The electrical conductivity (2000–2500 S cm^{-1}) and strength (0.5–0.6 GPa) of the tubular films significantly exceed those films consisting of CNT floccules or soot, which can be explained by the microstructural differences between these the CNT products (**Figure** 1c and **3**e and Figures S3 and S7, Supporting Information). The microscopic structure of tubular films comprises a continuous CNT network (Figure 3e). A CNT floccule consists of long CNT skeletons linked by many short CNTs, arising from failure of the C1 process in region II. A comparison of CNT aggregates from regions I and II (Figure S2, Supporting Information) illustrates the importance of C1 for successful CNT fabrication. In regions III and IV, an inadequate synthesis time leads to C2 failure and the primary products are sooted with isolated CNT bundles a few microns in length. Moreover, the tubular CNT films produced within the fabrication window, with the iron content of only ≈4 wt% as catalyst (Figure S4, Supporting Information), also have a higher purity than CNTs in other regions.

To further understand the BACVD method and demonstrate its scalability, we studied the blow-up ratio (BUR), defined as the ratio of the tubular film diameter (D_F) to the d. Figure 2d shows the variation of BUR versus gas flow for d ≈ 2.5 cm and different ITLs. BUR increases with increasing gas flow, but an inappropriate ITL can limit BUR. As D_F approaches the synthesis tube diameter, BUR changes slowly due to the restriction of the outer synthesis tube. BUR can be up to 4 with d ≈ 2.5 cm, and up to ≈6.7 with a fine inflation tube of d ≈ 1.5 cm (Videos S3 and S4, Supporting Information). Surprisingly, the permissible BUR range in BACVD is very wide. In contrast, the appropriate BUR in the blown plastic film method is rather limited (2.5–3.0).[10] Furthermore, it is worth mentioning that there is no hydrogen in the BACVD recipes, which made the CNT film preparation a very safe process. These results exhibit the flexibility of BACVD and the feasibility of large-scale production of CNT films.

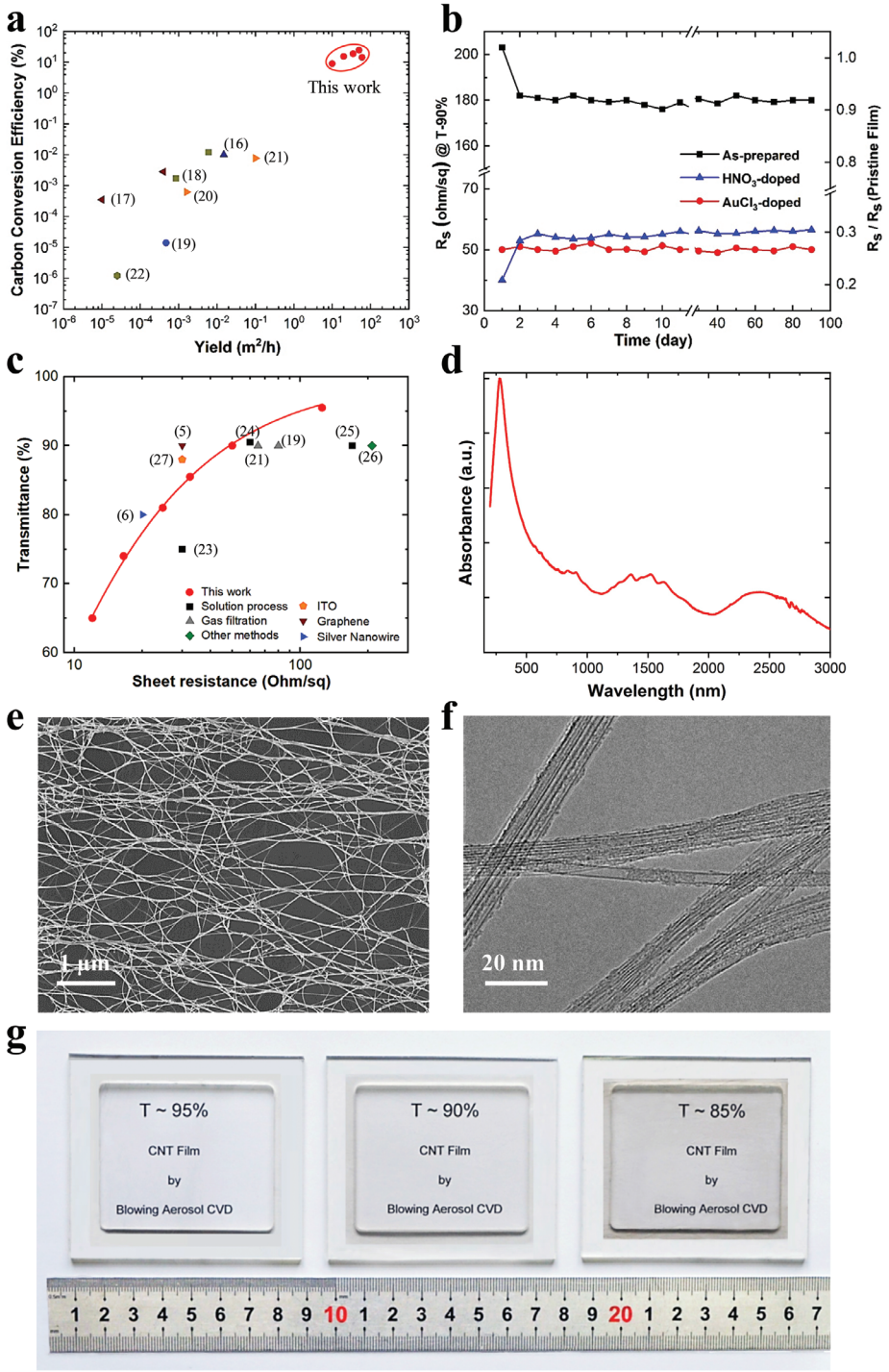

Figure 3. Characterization of the BACVD synthesized films as TCFs. a) Transparent SWCNT film yield and carbon conversion efficiency in BACVD, together with those FCCVD results reported previously (refs. [16–22]). b) Variation in and comparisons of R_s of pristine, $AuCl_3$-doped, and HNO_3-doped BACVD synthesized films under ambient conditions. The conductivity of the film improves by 3–4 times when doped by $AuCl_3$ or HNO_3. R_s changes in the first few days because of the spontaneous doping and de-doping of CNT films, then becomes extremely stable (relative change in resistance <5%). c) Sheet resistance versus transmittance of the $AuCl_3$-doped BACVD films. The best reported performance of large-area CNT films (over 100 cm^2) produced by other methods, that is, gas filtration based on FCCVD (refs. [19,21]), liquid process (refs. [23–25]), dry-drawing from multi-walled CNT forests (ref. [26]), and other large-area TCFs of ITO (ref. [27]), graphene (ref. [5]), and silver nanowire (ref. [6]) on flexible substrates, are shown for comparison. d) Optical absorption spectra of an as-synthesized pristine film, which is estimated to consist of SWCNTs with a mean diameter of around 2.2 nm. e) A typical SEM image of the BACVD synthesized film with 90% Tr, showing the continuous SWCNT bundle network and robust Y-type junctions formed at the growth temperature. f) A typical HRTEM image of the BACVD synthesized film, in which the SWCNT bundles are straight and homogeneous. g) Plexiglass frames covered by optically homogeneous and freestanding films with various transmittances.

For thin CNT film fabrication, in particular, BACVD exhibits an ultrahigh yield and high carbon conversion efficiency (the percentage of input carbon converted to CNTs). The yield of SWCNT film with 90% transmittance (Tr) can be over 50 m^2 h^{-1} and the carbon conversion efficiency can be as high as 25%. Both of them in BACVD are improved by up to three orders of magnitude over those in the reported works of SWCNT TCFs,[16–22] as shown in Figure 3a, which can greatly reduce the carbon emissions and energy consumptions in the SWCNT film fabrication.

The electrical properties of SWCNT films over a period of 90 days under ambient conditions demonstrate high stability (Figure 3b). For a Tr of 90%, the pristine SWCNT film shows a sheet resistance (R_s) of 180 Ω sq^{-1} and its conductivity can be improved 3–4-fold with HNO_3 or gold chloride ($AuCl_3$) doping. The best transparent conductivity observed was ≈40 Ω sq^{-1} in R_s at 90% Tr by HNO_3 doping, and the R_s deteriorated to 65 Ω sq^{-1} in two days. The change of R_s in the first few days results from spontaneous doping (the pristine films) and dedoping (HNO_3 doping) in air. With $AuCl_3$ doping, the R_s was around 50 Ω sq^{-1} at 90% Tr, and remained at this level even after three months lying aside in ambient conditions. Variation in R_s versus Tr of BACVD synthesized films with $AuCl_3$ doping, and comparisons of R_s with those of previously reported high-performance large-scale CNT films (over 100 cm^2) from gas filtration,[19,21] liquid-phase processing[23–25] and dry-drawing from CNT forests,[26] are shown in Figure 3c. So, relative to the samples reported so far in the literature, the stable R_s of 50 Ω sq^{-1} at 90% Tr of BACVD synthesized film represents the record performance of large-scale CNT films.[2,21] Moreover, the performance of BACVD film is similar to that of other large-scale TCFs (ITO,[27] graphene,[5] and silver nanowire[6]) on flexible substrates (Figure 3c).

The excellent transparency and conductivity, which determines whether the BACVD synthesized films could be applied as TCFs (Figure 3 and Section S4, Supporting Information), is primarily ascribed to the high-quality SWCNTs and the unique microstructures of the film. Optical absorption spectra (OAS) (Figure 3d) and Raman spectra (Figure S6, Supporting Information) indicate that the film is composed of SWCNTs with a mean diameter of ≈2.2 nm and good crystallinity (I_G/I_D = 75). According to scanning electron microscopy (SEM) and transmission electron microscopy (TEM) observations (Figure 3e,f and Figure S7, Supporting Information), the SWCNT films exhibit a continuously porous and reticulate microstructure with numerous Y-type junctions. These Y-type junctions form at high growth temperature and have longer inter-bundle connections, which benefits carrier transport.[16,28] In addition, we also propose that the ultralong SWCNTs that comprise the continuous BACVD synthesized films also contribute to high conductivity.[29] It is worth mentioning that the transmittance of freestanding CNT films, via BACVD, ranges from 97% to 60% and can be directly adjusted during film synthesis. The freestanding films of different transmittances mounted on plexiglass frames or poly(ethylene terephthalate) (PET) demonstrate their optical homogeneity (Figure 3g and Figure S9, Supporting Information).

The collection and storage of such a thin CNT film, especially one with transmittance >80%, are big challenges. A setup has been designed for direct and continuous collection of the BACVD synthesized film (**Figure 4**a,b and Video S5, Supporting Information), which is compatible with the general roll-to-roll process. Transparent electrodes can be obtained directly by using a transparent substrate such as PET or polyethylene (Figures S9 and S10, Supporting Information). Some low-surface-energy materials are also good flexible substrates, such as tracing papers. An ≈50 m long roll of the as-synthesized film on tracing paper is shown in Figure 4c. The magnified images in the insets of Figure 4c illustrate that the as-collected film is transparent and homogeneous. Especially, the as-collected CNT film can be directly peeled off as a freestanding film again, or can be transferred to some other target substrates (Figure 4d and Figure S11, Supporting Information). As shown in Figure 4e,f, the transparent, foldable, and stretchable electrodes are fabricated. For a foldable electrode fabrication, a CNT film of 90% transmittance is sandwiched between a transparent flexible tape and a piece of paper. Its resistance increases by only ≈3% with being folded (Figure 4e), and recovers when the film is returned to a flat state. The whole process of resistance variation-folding is reversible. The stretchable electrode is fabricated by a CNT film on a transparent polydimethylsiloxane (PDMS) film with a pre-elongation approach, as discussed in our previous work.[30] The PDMS film was pre-elongated to 200% and then released after the SWCNT film was transferred. With stretching, the resistance of the stretchable electrode near-linearly and slowly increases. As shown in Figure 4f, the variation of resistance is only ≈5% when the film is stretched to 160%.

In summary, we present an advanced BACVD technique as a new route for CNT assembly. By this method, a CNT aerosol is fabricated into the target form by being solidified into an aerogel during nanotube growth. A large-area, freestanding, and homogeneous SWCNT film with excellent transparency and conductivity has been synthesized directly and continuously by BACVD. Such film has considerable potential for applications as TCFs in flexible electronics, touch screens, photoresponsive sensors, and energy devices.[3,31] The high carbon conversion efficiency, ultrahigh extrusion yield, and stable controllability in composition and excellent performance of the as-synthesized films indicate that the BACVD method will be of great significance for the economical and high-throughput production of CNT films, especially as TCFs. Moreover, BACVD is compatible with roll-to-roll process, which could potentially be used in future high-throughput production of flexible displays, touch screens, solar cells, and solid-state lighting.[5,32]

Experimental Section

CNT Synthesis: Setting furnace temperature (T) at 1000 to ≈1200 °C, the feedstock and carrier gas were continuously fed into an inflation tube, and the auxiliary gas into a synthesis tube. A freestanding tubular CNT film was then continuously synthesized under these synthesis conditions in the fabrication window shown in Figure 2b, and was swept out of the equipment by the carrier and auxiliary gases. The feedstock comprised of catalyst, carbon source, and promoter. Methane acted as the carbon source, ferrocene as the catalyst, sulfur powder as the promoter, and nitrogen as the carrier and auxiliary gas. The carrier gas was used to blow and transport a bubble. Auxiliary gas was supplied in a small flow to remove the residual air and adjust the gas pressure.

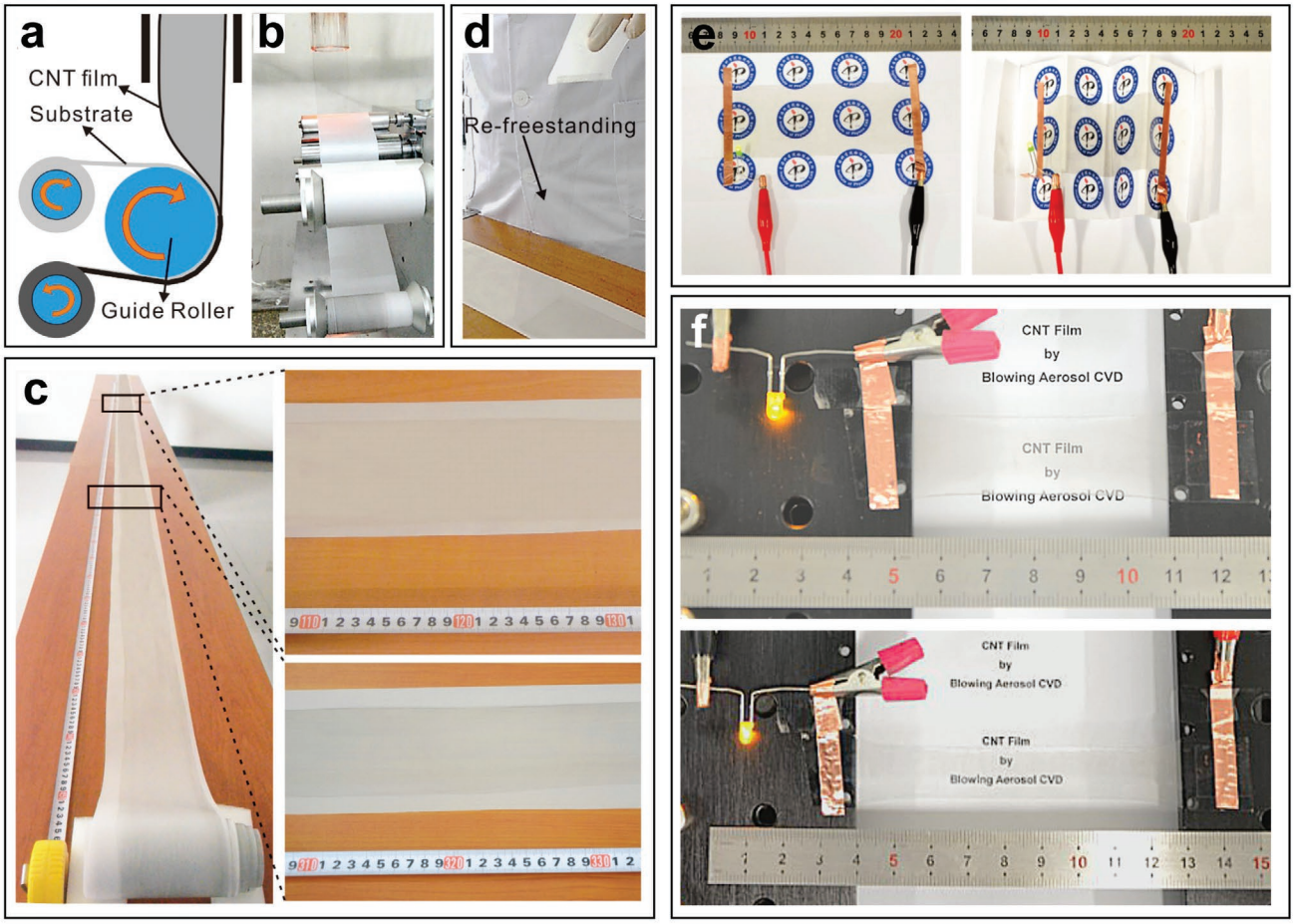

Figure 4. The continuous collection and applications of BACVD films. a) Schematic of a setup for continuous film collection on a flexible substrate. During collection, the tubular film is collapsed and attached to a flexible substrate over a guide roller. The composite structure composed of a CNT film and substrate is then collected on a winder. b) Photograph of the film collection on a tracing paper at ≈150 m h^{-1} for Equipment #2. c) Photograph of a ≈50 m long roll of the as-synthesized uniform film (≈10 cm width) on a tracing paper and magnified photographs of the framed regions. d) Freestanding film re-obtained by directly peeling off the tracing paper. e) Photographs of transparent, foldable electrodes. An ultrathin CNT film is sandwiched between a transparent flexible tape and a piece of paper with special logos. Here, its resistance increases by about 3% after being folded. f) Photographs of a LED illuminated using a transparent CNT/PDMS film as the connection part without (above) and with (below) an elongation. The resistance increases by ≈5% during the film is stretched to 160%.

Specific synthesis conditions for the growth of tubular films by BACVD are given as follows:

For small scale Equipment #1, 0 to ≈0.2 standard liters per min (slm) of nitrogen was used as the auxiliary gas, and 5 to ≈30 standard cubic centimeters per min (sccm) of methane, and a 1 to ≈5 mg min^{-1} mixture of ferrocene and sulfur powder (mole ratio of Fe:S from 2 to 8) were introduced by a carrier gas (0.2 to ≈1.2 slm of nitrogen).

For large-scale Equipment #2, 0 to ≈0.4 slm of nitrogen was used as the auxiliary gas, and 10 to ≈60 sccm of methane, and a 6 to ≈10 mg min^{-1} mixture of ferrocene and sulfur powder (mole ratio of Fe:S from 2 to 8) were introduced by a carrier gas (0.6 to ≈4 slm of nitrogen).

The general phase diagram of CNTs produced by BACVD was determined, according to success or failure of process C1 or C2 under a given synthesis condition. For Equipment 2, the inflation tube was gradually moved ≈5 cm down the reactor axis while the gas flow was gradually increased ≈0.2 slm at each specific position of the inflation tube outlet. Besides, more data points were observed to supplement and verify the proposed phase diagram. For each specific ITL and gas flow, both the process of blown bubble at the inflation tube outlet and final products at the outlet of synthesis tube were observed. The minimum value of carrier gas flow was 0.8 slm. A wide variety of CNT products resulting from the changes in the carrier gas flow and the ITL were investigated. Then four zones were determined based on the observation and systematic analysis of data points. Moreover, a similar phase diagram of four zones could be built for Equipment 1 with ITL movement of ≈2 cm and gas flow increase of ≈0.1 slm.

CNT Films as TCFs: The as-synthesized freestanding CNT films were directly transferred onto PET films, as transparent electrodes. Ethanol was then dripped onto the film for densification. The CNT films were doped by HNO_3 or $AuCl_3$ to improve their conductivity. For HNO_3 doping, the CNT films were immersed in a 67% HNO_3 solution for 30 min followed by rinsing with deionized water and N_2 drying. For $AuCl_3$ doping, the films were treated with 16 mM solution of $AuCl_3$ in acetonitrile by the drop-casting technique. After doping for 3 min, the films were washed with pure acetonitrile followed by N_2 drying.

Sheet resistances of the CNT TCFs were measured using a four-point probe (Jandel Engineering Ltd, UK, tip radius 250 µm, tip spacing 1 mm) connected to a multi-meter (HP/Hewlett Packard 3485A). The plot of T versus R_s was nonlinearly fitted based on methods described in the literature.

Characterization: Optical images and videos were recorded by a digital camera (Nikon, D7000). A mirror close to the synthesis outlet was used to monitor the blown bubble process.

The morphology and microstructures of the CNT products were characterized by SEM (Hitachi 4800 and S5200) and TEM (Tecnai F20 and JEOL JEM-2010). Raman scattering spectra were recorded by LabRAM HR800 (HORIBA Jobin Yvon Inc.) with excitation lasers of 514, 633, and 785 nm wavelengths. For optical characterizations, CNT films were collected on transparent quartz slides. OAS and transmittance of the SWCNTs films were measured using an Agilent Carry 5000 UV–vis–NIR spectrometer (Agilent Technologies, Inc.).

The electrical and mechanical properties and purity of CNT products from various regions were assessed based on CNT films around 500 nm in thickness. The tubular films and CNT floccules were directly spun up. The CNT soot was deposited on the inner wall of the synthesis tube and then peeled off. Film resistances were measured by a Keithley-2400 SourceMeter with the four-terminal method under a current of 0.1 mA, using a sample with a width of 20 mm and a gauge length of 50 mm. Mechanical properties were measured using a dynamic mechanical analyzer (Q800, TA Instruments) at a tensile speed of 0.05 mm min^{-1}. The samples were cut into strips with a width of 3 mm, pasted onto a hollow card mount with a gauge length of 15 mm for these measurements. The thermal stability of the films and the amount of catalyst residues were examined by detecting the weight loss of a sample as temperature increases with a set ramp over a given period of time (Thermo gravimetric analyzer Q500, TA Instruments). In thermo gravimetric analysis tests, the sample was placed in a ceramic crucible and heated up from room temperature to 1000 °C at a rate of 10 °C min^{-1} in dry air of 100 sccm. Film thickness was measured by a stylus profiler (Dektak XT, Bruker). All films were densified by ethanol before the thickness measurement. For a thick film, its thickness (with over 100 nm in thickness or corresponding transmittance <60%, normally) was measured directly. For a thinner film, the thickness was averaged over multiple layers to reduce measuring error.

Carbon conversion efficiency was calculated based on carbon input from carbon source and CNT film weight. A SWCNT could be thought of as a sheet of graphene rolled into a cylinder. The areal density of a SWCNT film with a Tr of 90% was considered to be the same as that of a 4.5-layer graphene. Then the mass of SWCNT film could be calculated. Moreover, the mass of tubular CNT films continuously collected in a certain time was measured with a high precision balance (METTLER TOLEDO XP2U, readability 0.2 µg). The weighing result was consistent with the calculation result.

Supporting Information

Supporting Information is available from the Wiley Online Library or from the author.

Acknowledgements

This work was financially supported by the National Key R&D Program of China (Grant No. 2018YFA0208402), the National Natural Science Foundation of China (11634014, 51172271, and 51372269), the "Strategic Priority Research Program" of the Chinese Academy of Sciences (XDA09040202), the National Basic Research Program of China (Grant No. 2012CB932302). The authors thank L. A. Wu, G. H. Rao, and M. Jones for valuable advice on the manuscript; X.A. Yang, L.N. Zhang, and X.Y. Qi for their assistance in characterization using transmission electron microscopy; and H. P. Liu for transmittance test.

Conflict of Interest

The authors declare no conflict of interest.

Keywords

blown aerosol technique, carbon nanotubes, high yield, roll-to-roll, transparent conductive films

Received: June 23, 2020
Revised: July 23, 2020
Published online:

[1] K. Ellmer, *Nat. Photonics* **2012**, *6*, 809.
[2] L. Yu, C. Shearer, J. Shapter, *Chem. Rev.* **2016**, *116*, 13413.
[3] L. Hu, D. S. Hecht, G. Grüner, *Chem. Rev.* **2010**, *110*, 5790.
[4] A. G. Nasibulin, A. Kaskela, K. Mustonen, A. S. Anisimov, V. Ruiz, S. Kivist, S. Rackauskas, M. Y. Timmermans, M. Pudas, B. Aitchison, M. Kauppinen, D. P. Brown, O. G. Okhotnikov, E. I. Kauppinen, *ACS Nano* **2011**, *5*, 3214.
[5] S. Bae, H. Kim, Y. Lee, X. Xu, J. S. Park, Y. Zheng, J. Balakrishnan, T. Lei, H. Ri Kim, Y. Il Song, Y. J. Kim, K. S. Kim, B. Özyilmaz, J. H. Ahn, B. H. Hong, S. Iijima, *Nat. Nanotechnol.* **2010**, *5*, 574.
[6] L. Hu, H. S. Kim, J. Y. Lee, P. Peumans, Y. Cui, *ACS Nano* **2010**, *4*, 2955.
[7] H. Wu, L. Hu, M. W. Rowell, D. Kong, J. J. Cha, J. R. McDonough, J. Zhu, Y. Yang, M. D. McGehee, Y. Cui, *Nano Lett.* **2010**, *10*, 4242.
[8] Q. Zhang, N. Wei, P. Laiho, E. I. Kauppinen, *Top. Curr. Chem.* **2017**, *375*, 90.
[9] L. H. Sperling, *Introduction to Physical Polymer Science*, 4th ed., John Wiley & Sons, Chichester, UK **2006**.
[10] T. Kanai, *IEEE Electr. Insul. Mag.* **2001**, *17*, 59.
[11] Y. Li, I. A. Kinloch, A. H. Windle, *Science* **2004**, *304*, 276.
[12] A. G. Nasibulin, P. V. Pikhitsa, H. Jiang, D. P. Brown, A. V. Krasheninnikov, A. S. Anisimov, P. Queipo, A. Moisala, D. Gonzalez, G. Lientschnig, A. Hassanien, S. D. Shandakov, G. Lolli, D. E. Resasco, M. Choi, D. Tománek, E. I. Kauppinen, *Nat. Nanotechnol.* **2007**, *2*, 156.
[13] A. M. Boies, C. Hoecker, A. Bhalerao, N. Kateris, J. de La Verpilliere, B. Graves, F. Smail, *Small* **2019**, *15*, 1900520.
[14] P. Kulkarni, P. A. Baron, K. Willeke, Eds, *Aerosol Measurement: Principles, Techniques, and Applications*, 3rd ed., John Wiley & Sons, Chichester, UK **2011**.
[15] L. Hu, D. S. Hecht, G. Grüner, *Nano Lett.* **2004**, *4*, 2513.
[16] W. Ma, L. Song, R. Yang, T. Zhang, Y. Zhao, L. Sun, Y. Ren, D. Liu, L. Liu, J. Shen, Z. Zhang, Y. Xiang, W. Zhou, S. S. Xie, *Nano Lett.* **2007**, *7*, 2307.
[17] A. Hussain, Y. Liao, Q. Zhang, E. X. Ding, P. Laiho, S. Ahmad, N. Wei, Y. Tian, H. Jiang, E. I. Kauppinen, *Nanoscale* **2018**, *10*, 9752.
[18] E. X. Ding, H. Jiang, Q. Zhang, Y. Tian, P. Laiho, A. Hussain, Y. Liao, N. Wei, E. I. Kauppinen, *Nanoscale* **2017**, *9*, 17601.
[19] Y. Liao, A. Hussain, P. Laiho, Q. Zhang, Y. Tian, N. Wei, E. X. Ding, S. A. Khan, N. N. Nguyen, S. Ahmad, E. I. Kauppinen, *Adv. Mater. Interfaces* **2018**, *5*, 1801209.
[20] S. Jiang, P. Hou, M. Chen, Q. Guo, D. Tang, D. D. Zhang, B. W. Wang, D. Sun, Q. Jin, J. Du, K. Tai, J. Tan, E. I. Kauppinen, C. Liu, H. Cheng, *Sci. Adv.* **2018**, *4*, 9264.
[21] B. W. Wang, S. Jiang, Q. B. Zhu, Y. Sun, J. Luan, P. X. Hou, S. Qiu, Q. W. Li, C. Liu, D. M. Sun, H. M. Cheng, *Adv. Mater.* **2018**, *30*, 1802057.
[22] K. Mustonen, P. Laiho, A. Kaskela, Z. Zhu, O. Reynaud, N. Houbenov, Y. Tian, T. Susi, H. Jiang, A. G. Nasibulin, E. I. Kauppinen, *Appl. Phys. Lett.* **2015**, *107*, 013106.
[23] Z. Wu, Z. Chen, X. Du, J. M. Logan, J. Sippel, M. Nikolou, K. Kamaras, J. R. Reynolds, D. B. Tanner, A. F. Hebard, A. G. Rinzler, *Science* **2004**, *305*, 1273.
[24] B. Dan, G. C. Irvin, M. Pasquali, *ACS Nano* **2009**, *3*, 835.

[25] H. Z. Geng, K. K. Kim, K. P. So, Y. S. H. Lee, Y. Chang, Y. S. H. Lee, *J. Am. Chem. Soc.* **2007**, *129*, 7758.
[26] C. Feng, K. Liu, J. S. Wu, L. Liu, J. S. Cheng, Y. Zhang, Y. Sun, Q. Li, S. Fan, K. Jiang, *Adv. Funct. Mater.* **2010**, *20*, 885.
[27] S. I. Kim, K. W. Lee, B. B. Sahu, J. G. Han, *Jpn. J. Appl. Phys.* **2015**, *54*, 090301.
[28] D. Sun, M. Y. Timmermans, Y. Tian, A. G. Nasibulin, E. I. Kauppinen, S. Kishimoto, T. Mizutani, Y. Ohno, *Nat. Nanotechnol.* **2011**, *6*, 156.
[29] N. Behabtu, C. C. Young, D. E. Tsentalovich, O. Kleinerman, X. Wang, A. W. K. Ma, E. A. Bengio, R. F. ter Waarbeek, J. J. de Jong, R. E. Hoogerwerf, S. B. Fairchild, J. B. Ferguson, B. Maruyama, J. Kono, Y. Talmon, Y. Cohen, M. J. Otto, M. Pasquali, *Science* **2013**, *339*, 182.
[30] N. Zhang, P. Luan, W. Zhou, Q. Zhang, L. Cai, X. Zhang, W. Zhou, Q. Fan, F. Yang, D. Zhao, Y. Wang, S. Xie, *Nano Res.* **2014**, *7*, 1680.
[31] M. F. L. De Volder, S. H. Tawfick, R. H. Baughman, A. J. Hart, *Science* **2013**, *339*, 535.
[32] C. E. Small, S. Chen, J. Subbiah, C. M. Amb, S. W. Tsang, T. H. Lai, J. R. Reynolds, F. So, *Nat. Photonics* **2012**, *6*, 115.